

# Monodisperse patchy particle glass former

Cite as: J. Chem. Phys. **154**, 174501 (2021); <https://doi.org/10.1063/5.0036963>

Submitted: 09 November 2020 . Accepted: 14 April 2021 . Published Online: 03 May 2021

 Susana Marín-Aguilar,  Frank Smallenburg,  Francesco Sciortino, and  Giuseppe Foffi



View Online



Export Citation



CrossMark

## ARTICLES YOU MAY BE INTERESTED IN

[Dynamical properties of different models of elastic polymer rings: Confirming the link between deformation and fragility](#)

The Journal of Chemical Physics **154**, 154901 (2021); <https://doi.org/10.1063/5.0041264>

[Phase separation in mixed suspensions of bacteria and nonadsorbing polymers](#)

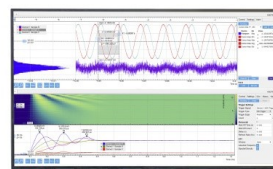
The Journal of Chemical Physics **154**, 151101 (2021); <https://doi.org/10.1063/5.0045435>

[Dynamical phase transitions and their relation to structural and thermodynamic aspects of glass physics](#)

The Journal of Chemical Physics **153**, 090901 (2020); <https://doi.org/10.1063/5.0006998>

Challenge us.

What are your needs for  
periodic signal detection?



Zurich  
Instruments



# Monodisperse patchy particle glass former

Cite as: *J. Chem. Phys.* **154**, 174501 (2021); doi: [10.1063/5.0036963](https://doi.org/10.1063/5.0036963)

Submitted: 9 November 2020 • Accepted: 14 April 2021 •

Published Online: 3 May 2021



View Online



Export Citation



CrossMark

Susana Marín-Aguilar,<sup>1,a)</sup>  Frank Smallenburg,<sup>1,b)</sup>  Francesco Sciortino,<sup>2</sup>  and Giuseppe Foffi<sup>1,c)</sup> 

## AFFILIATIONS

<sup>1</sup>Université Paris-Saclay, CNRS, Laboratoire de Physique des Solides, 91405 Orsay, France

<sup>2</sup>Department of Physics, Sapienza University of Rome, P.le Aldo Moro 5, 00185 Rome, Italy

<sup>a)</sup> Author to whom correspondence should be addressed: [susana.marin-aguilar@universite-paris-saclay.fr](mailto:susana.marin-aguilar@universite-paris-saclay.fr)

<sup>b)</sup> Electronic mail: [frank.smallenburg@universite-paris-saclay.fr](mailto:frank.smallenburg@universite-paris-saclay.fr)

<sup>c)</sup> Electronic mail: [giuseppe.foffi@universite-paris-saclay.fr](mailto:giuseppe.foffi@universite-paris-saclay.fr)

## ABSTRACT

Glass formers are characterized by their ability to avoid crystallization. As monodisperse systems tend to rapidly crystallize, the most common glass formers in simulations are systems composed of mixtures of particles with different sizes. Here, we make use of the ability of patchy particles to change their local structure to propose them as monodisperse glass formers. We explore monodisperse systems with two patch geometries: a 12-patch geometry that enhances the formation of icosahedral clusters and an 8-patch geometry that does not appear to strongly favor any particular local structure. We show that both geometries avoid crystallization and present glassy features at low temperatures. However, the 8-patch geometry better preserves the structure of a simple liquid at a wide range of temperatures and packing fractions, making it a good candidate for a monodisperse glass former.

Published under license by AIP Publishing. <https://doi.org/10.1063/5.0036963>

## I. INTRODUCTION

When a fluid is subjected to extreme conditions of low temperatures or high densities but manages to avoid crystallization, its dynamics become glassy. In this glassy regime, the system is structurally similar to a liquid, in which it lacks long-range order, but the relaxation of the system occurs over much longer time scales due to the increasing difficulty in performing local rearrangements. For purely repulsive particles, for example, we can picture this difficulty as coming from particles being strongly confined to their positions by the cage of neighbors formed around them.

To reach the glassy regime, a glass former needs to remain disordered, which is usually unfavorable compared to crystallization at sufficiently low temperatures. A good glass former, then, is a system that can be deeply cooled down, to the point where dynamics become extremely slow, while reliably avoiding crystal formation. Different methods have been proposed to enhance the ability of a system to avoid crystallization. For example, in Ref. 1, three routes for the design of an optimal glass former system were proposed: a kinetic, a thermodynamic, and a topological route. The kinetic one aims at slowing down the crystal nucleation rate: even if a fluid is metastable with respect to the crystal (and hence supercooled), when the typical nucleation time is much longer than the time scale of

the experiment or simulation, crystallization is effectively avoided. The thermodynamic route suggests acting on the thermodynamically stability field of the crystal by shifting it to more extreme conditions of temperature and density. This can be done, for example, by tuning the composition of a binary mixture to create a eutectic mixture, with a freezing temperature that is lower than any other composition.<sup>2,3</sup> Similarly, for network glasses, valence can be used to destabilize the crystal phase.<sup>4</sup> Following this route, an ideal glass former would have a melting point located below its glass transition temperature.<sup>5</sup> Finally, the topological mechanism relies on reinforcing local structures that are incompatible with crystal lattices and cannot be replicated in three-dimensions leading to geometrical frustration.<sup>6,7</sup> This is done by modifying the interaction between the components of the system or by changing the shape of the particles.<sup>1,6</sup> In practice, this last route will overlap with the other two, as changing interactions to favor different local structures will invariable also impact the thermodynamics and kinetics of the system. However, it does represent a very promising route to design a good glass former, which we will draw on in this work.

Most simulation studies of supercooled liquids rely on the use of mixtures of particles of different sizes in order to avoid crystallization.<sup>8–10</sup>

However, while multicomponent or polydisperse systems have been the most common subjects of simulation studies in glass physics, it is clear that a monodisperse model would represent a more ideal testing ground. For example, detailed mode-coupling theory (MCT) predictions have been developed for monodisperse cases,<sup>11</sup> but the window in which it was possible to test this prediction in a real monoatomic case is strongly limited.<sup>12</sup> Clearly, MCT predictions have been generalized to mixtures,<sup>13</sup> but non-trivial mixing effects can alter the dynamics.<sup>14</sup> In general, binary (and multicomponent) systems display thermodynamic fluctuations in both density and concentration, and this can have important consequences for the dynamics. For instance, as the different species typically have different diffusion constants, we can expect different dynamical behavior for each component. Recently, it has also been shown that the interplay between mass diffusion and concentration diffusion could result in effects that are specific to mixtures and are not observed in monodisperse glass formers.<sup>15</sup> Although these effects may be weaker in systems with a continuous size distribution, polydisperse systems can lead to crystallization effects facilitated by size segregation. This may also affect the dynamics of the system in ways that are still to be completely grasped.<sup>16</sup>

Metallic glasses are generally obtained in multicomponent melts, and it was only recently that monodisperse glasses have been experimentally obtained.<sup>17,18</sup> In fact, the observation of a monoatomic metallic glass was realized in part, thanks to a model introduced to suppress crystallization.<sup>19</sup> Since the seminal work of Pusey and van Meegen, colloidal hard spheres have become one of the gold standards in testing glass theories.<sup>20–22</sup> However, monodisperse hard spheres undergo crystallization well before their dynamics become glassy. It is now well established that a polydispersity of around 10% is needed to avoid crystallization.<sup>23</sup> For practical reasons, this is the route that is typically followed in experiments, while in computer simulations, binary mixtures of hard spheres with different radii are more commonly used.

If we want to avoid the use of multicomponent mixtures, the topological route to avoid crystallization suggests tuning the interactions such that the locally favored structures are incommensurate with crystallization. Indeed, it has been found that carefully designed interactions in monodisperse systems can suppress crystallization in the fluid.<sup>6,19,24</sup> This can be achieved by adding many-body interactions to the potential<sup>17,19,24</sup> or with oscillatory interactions.<sup>25–31</sup> In particular, these potentials are designed to promote local structures that are typically icosahedral<sup>25–27</sup> or tetrahedral<sup>17,19,29</sup> motifs that cannot be used to tile an infinite three dimensional space. However, both many-body interactions and oscillatory interaction potentials are difficult to tune in experimental setups of, for example, colloidal particles. Here, we draw inspiration from recent advances in colloid synthesis<sup>32–34</sup> and focus on systems of patchy particles: spherical particles with a limited number of attractive spots on the surface.

The idea of using patchy particles as a monodisperse glass former is based on the observation that patchy particles have proven to be a great tool for exploring and controlling the interplay between the local structure and dynamics of supercooled liquids<sup>35,36</sup> and gels.<sup>37</sup> We will show that the directionality embedded in the interaction potential is capable of drastically modifying the local structure of the fluid, which aids in avoiding crystallization. In particular, it has been shown previously that in binary mixtures of patchy

particles with an icosahedral geometry, the number of icosahedral local structures in the system is boosted with a consequent slowdown of dynamics.<sup>35</sup> This geometry, however, might result in a local order that is not representative of a typical liquid structure. Therefore, we have also investigated the 8-patch case, a geometry that still aids in avoiding crystallization but does not impact the fluid structure to the same degree. We propose that this 8-patch model is therefore a good candidate for a monodisperse glass former.

This paper is organized as follows: In Sec. II, we describe the model we use to simulate patchy particles and the details of the simulations. In Sec. III, we compare the crystallization behavior of our patchy-particle systems with that of a monodisperse square-well system and show that both geometries are capable of avoiding crystallization at low temperatures. Since the 8-patch geometry better conserves the structure of a simple liquid, from there we move to a detailed characterization of the structural and the dynamical behavior of the 8-patch case at different temperatures and packing fractions. We finish Sec. III by discussing the nature of the relaxation behavior of this particular geometry. Finally, in Sec. IV, we conclude and summarize the main results of this paper.

## II. METHODS

### A. Model

To simulate patchy particles, we use the Kern–Frenkel model.<sup>38</sup> This model consists of hard-sphere particles decorated with  $n$  attractive patches on their surface. Two particles interact attractively, with a fixed bonding energy  $\epsilon$ , when the vector that joins their centers passes through a patch in each particle. Hence, the interaction potential is given by

$$U_{ij} = U^{HS} + \sum_{\alpha} \sum_{\gamma} U^{SW} f(\mathbf{r}_{ij}, \hat{\mathbf{n}}_{\alpha}, \hat{\mathbf{n}}_{\gamma}), \quad (1)$$

where the sums are taken over all patches  $\alpha$  and  $\gamma$  of the two particles. Additionally,  $U^{HS}$  is the hard-sphere potential,

$$U_{ij}^{HS} = \begin{cases} \infty, & r_{ij} \leq \sigma \\ 0, & r_{ij} > \sigma, \end{cases} \quad (2)$$

and  $U^{SW}$  corresponds to a square-well potential,

$$U_{ij}^{SW} = \begin{cases} -\epsilon, & r_{ij} \leq r_c \\ 0, & r_{ij} > r_c, \end{cases} \quad (3)$$

where  $\sigma$  is the particle diameter,  $r_{ij}$  is the distance between two particles  $i$  and  $j$ ,  $r_c$  is the interaction range, and  $\epsilon$  is the strength of the attraction. Finally,  $f(\mathbf{r}_{ij}, \hat{\mathbf{n}}_{\alpha}, \hat{\mathbf{n}}_{\beta})$  takes a value of 1 when two patches are face to face and 0 otherwise, where  $\hat{\mathbf{n}}_{\alpha(\gamma)}$  denotes the direction of a patch  $\alpha(\gamma)$  in each particle. Specifically, two patches are considered to be facing each other when for both patches, the angle between  $\hat{\mathbf{n}}$  and the vector connecting the centers of two particles is smaller than the patch opening angle  $\theta$ . Finally, we define the fraction of the surface covered by the patches as  $\chi$ . As long as patches do not overlap,  $\chi = n(1 - \cos \theta)/2$ , with  $n$  being the number of patches.

We model two cases: particles with  $n = 8$  and 12 patches. We choose the location of the patches on the surface of the particle such that the distance between them is maximized. This corresponds to

the vertices of a square antiprism<sup>39</sup> for the former case and an icosahedron for the latter. Following Ref. 7, we fix the surface coverage  $\chi = 40\%$  and cutoff radius  $r_c = 1.031\sigma$  for both systems. The short interaction range is chosen partially to allow for easy comparison with earlier work on binary mixtures<sup>7,40,41</sup> and partially to be compatible with the typical short-range interactions found in experimental realizations of patchy colloids.<sup>42–44</sup>

## B. Simulation

We use event-driven molecular dynamics (EDMD) simulations<sup>4</sup> to explore monodisperse systems of patchy particles. Each system consists of  $N = 700$  particles, and we initially fix the packing fraction  $\eta = \frac{\pi}{6}\rho\sigma^3 = 0.56$ . Additionally, we explore the behavior of the 8-patch case at higher packing fractions  $\eta = 0.57$  and  $0.58$ . Finally, as a reference point, we simulate a monodisperse system of purely square-well particles with the same attractive range as the patchy particle systems, at the same state points.

We present our results in reduced units, where the  $\sigma$  is the unit of length,  $\varepsilon$  is the unit of energy, and the particle mass  $m$  is the unit of mass. Moreover, we set  $k_B = 1$ . With this choice of units, the unit of time is  $\tau = \sigma\sqrt{m/\varepsilon}$ . We start each simulation from an initial configuration that was generated from an EDMD simulation of  $N$  hard spheres where the particles start off much smaller than their final size but rapidly grow with time until a disordered configuration at the desired packing fraction is reached. Subsequently, we equilibrate the systems at fixed temperature for at least  $t = 10^4$  and finally perform our measurements over simulations of at least  $t = 10^5$ .

In addition to EDMD simulations, we also make use of Floppy Box Monte Carlo (FBMC) simulations to check for the possibility of fully bonded crystal structures in the 8-patch model.<sup>45</sup> This method has proven effective at finding optimal packings and ground states for a variety of model systems, including patchy particles.<sup>46,47</sup> Specifically, we simulate a single unit cell containing up to 12 particles in a periodic box whose shape is allowed to vary during the simulation. By slowly reducing the temperature, the system is annealed into a highly bonded state. We perform this simulation 20 times for system sizes  $N \in 1, \dots, 12$  and a range of choices for the ratio between pressure at temperature ( $P/T$ ). The resulting library of annealed snapshots provides a set of candidate structures for the ground state of our model.

Finally, to calculate the gas–liquid critical point and the gas–liquid coexistence, we use successive umbrella sampling,<sup>48</sup> previously applied to study the phase coexistence of numerous patchy particle models<sup>49,50</sup> as well as particles interacting with strong directional interactions.<sup>51,52</sup> Specifically, the box size was fixed to  $9\sigma$  along all three dimensions, and the density fluctuations were calculated splicing together 700 independent grand-canonical simulations, in which the number of particles was constrained to fluctuate between  $N$  and  $N + 1$ , with  $N = 0, \dots, 699$ .

## C. Analysis

We characterize the global structure of each system via the static structure factor,

$$S(q) = \frac{1}{N} \langle \rho(-\mathbf{q}, t) \rho(\mathbf{q}, t) \rangle, \quad (4)$$

where  $\rho(\mathbf{q}, t)$  is the Fourier component of the microscopic density at time  $t$  for a given wave vector  $\mathbf{q}$ . The average is performed over snapshots taken at different times in the same simulation.

To detect crystallization in our system, we also calculate the structure factor  $S(\mathbf{q})$  in the  $xy$ -plane. This projection, equivalent to the measured pattern in a small angle scattering experiment, gives a clear blueprint of the structure. For a homogeneous liquid, we find an arrangement of rings corresponding to the isotropic and homogeneous structure of the sample, while a crystallized system shows well-defined peaks reflecting the anisotropy of the structure. In addition to the structure factor, an extra indicator of the phase is the bond orientational order parameters.<sup>53,54</sup> These order parameters characterize the environment of each particle, based on its nearest neighbors. As we are primarily concerned with crystallization into close-packed lattices, we focus here on the sixfold order parameter  $Q_6$ . This quantity is defined as

$$Q_6(i) = \sqrt{\frac{4\pi}{13} \sum_{m=-6}^6 |\bar{Q}_{6m}(i)|^2}, \quad (5)$$

where

$$\bar{Q}_{6m}(i) = \frac{1}{N_b} \sum_{j=1}^{N_b} Y_{6m}(\theta(\mathbf{r}_{ij}), \phi(\mathbf{r}_{ij})), \quad (6)$$

where the sum is taken over all  $N_b$  the neighbors of particle  $i$ .  $Y_{6m}$  are the spherical harmonics of order 6, and  $\theta(\mathbf{r}_{ij})$  and  $\phi(\mathbf{r}_{ij})$  are the polar and azimuthal angle associated with the vector  $\mathbf{r}_{ij}$  connecting particles  $i$  and  $j$ .<sup>53,54</sup> The global average  $Q_6$  of this bond order parameter, taken over all particles in the system, then gives an indication of the crystalline order in the system. For a perfect face-centered cubic (fcc) lattice,  $Q_6 = 0.57452$ , and for a perfect hexagonal close-packed (HCP) lattice,  $Q_6 = 0.48476$ , while typical values in the fluid phase are much lower.<sup>53,54</sup> Crystallization of the system is accompanied by a discontinuous jump in  $Q_6$  across the transition.

In order to characterize the local environment of particles, we also use the *topological cluster classification* algorithm.<sup>55</sup> This algorithm defines a set of nearest neighbors for each particle based on a modified Voronoi construction and subsequently uses these nearest-neighbor bonds to identify predefined local clusters, ranging from simple clusters of three particles to more complex clusters of up to 13 particles. In this paper, we focus, in particular, on icosahedral and defective icosahedral clusters that have proven to play an important role in supercooled liquids.<sup>7,56–58</sup>

We explore the glassy dynamics of our systems by calculating the mean-square displacement (MSD) as  $\langle r^2 \rangle = \frac{1}{N} \langle \sum_{i=1}^N [\mathbf{r}_i(t) - \mathbf{r}_i(0)]^2 \rangle$ , where the average is performed on equilibrium trajectories. Additionally, to quantify the structural relaxation time of our systems, we calculate the time-dependent intermediate scattering function (ISF),

$$F(q, t) = \frac{\langle \rho(-\mathbf{q}, t) \rho(\mathbf{q}, 0) \rangle}{\langle \rho(-\mathbf{q}, 0) \rho(\mathbf{q}, 0) \rangle}. \quad (7)$$

We extract a relaxation time from the long time decay of  $F(q, t)$  by fitting it with a sum of two stretched exponential functions,

$$f(t) = (1 - f_q) \exp\left[-\left(\frac{t}{\tau_a}\right)^{\gamma_a}\right] + f_q \exp\left[-\left(\frac{t}{\tau_b}\right)^{\gamma_b}\right], \quad (8)$$

where  $f_q$ ,  $\gamma_{a(b)}$ , and  $\tau_{a(b)}$  are fitting parameters. This procedure is also used to identify the non-ergodicity parameter  $f_q$ . We define the relaxation time  $\tau_{0.3}$  as the time where  $F(q, t)$  has decayed to  $0.3f_q$ .

### III. RESULTS

#### A. Square well

As a starting point, we explore the behavior of a monodisperse short-range square-well (SW) system with a fixed packing fraction  $\eta = 0.56$ . As discussed below, the SW model has been studied in great detail in the literature, and the purpose of this section is solely to have a benchmark case for the original results that we will discuss in the rest of this paper. This will allow us to compare our patchy-particle models directly to a similar monodisperse system with isotropic interactions.

Square-well models with short interaction ranges have been studied extensively in the past as they represent a good model for colloidal systems. They have a phase diagram that differs from the typical van der Waals picture, showing a metastable liquid–liquid phase separation<sup>59</sup> and an isostructural solid–solid transition.<sup>60</sup> From the dynamical point of view, they are known to show reentrant behavior in both their dynamics and crystallization as a function of temperature.<sup>41,60–65</sup> In particular, a number of studies have demonstrated reentrant dynamical behavior resulting from a crossover between an attractive and a repulsive glass. Although both of these glass states are arrested, the mechanism driving the arrest is different. At high temperatures, the arrest is mainly due to the high packing fraction of the system, while at low temperatures, attractions dominate. In between these regimes, the attractive interactions are not yet strong enough to drive arrest but do help to reduce the pressure, recovering some freedom of movement for the particles and hence speeding up dynamics.

A similar mechanism affects crystallization. Upon lowering the temperature, the crystal transform from being relatively loosely packed, with few bonds, to a tightly bound crystal where particles are within the bonding range of their neighbors. At intermediate temperatures, the crystal phase is less favored, opening up a window where crystallization is more difficult.<sup>60</sup> To see how this affects spontaneous crystallization, we plot in Fig. 1 the behavior of the bond order parameter  $Q_6$  as a function of temperature for the square-well system. At high temperatures, the system readily crystallizes into an fcc crystal, as indicated by the high values of  $Q_6$ . Note that the spontaneous crystallization typically results in the presence of grain boundaries and other defects, which tend to decrease  $Q_6$ . At lower temperatures (yellow region in Fig. 1), crystallization is avoided, resulting in a glassy disordered state. At even lower temperatures, we again observe crystallization, favored by the strong attractions. In this regime, the resulting crystal phase is packed more densely than the original system to accommodate strong bonding between the particles, resulting in a coexistence with a lower-density fluid or gas.<sup>66</sup> This is seen most clearly at the lowest temperature investigated and illustrated in the snapshot in Fig. 1.

It is important to note here that we rely on spontaneous crystallization here to determine the phase behavior. Hence, even in the

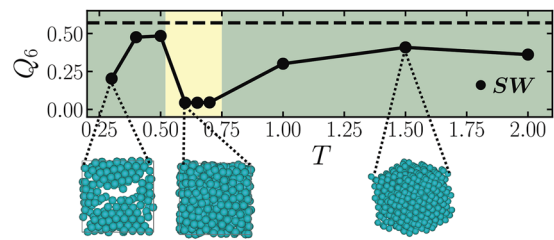


**FIG. 1.**  $Q_6$  as a function of temperature for a monodisperse system of square well at the packing fraction  $\eta = 0.56$ . Yellow regions correspond to a fluid phase, and green regions to a crystallized phase. The dashed line is the  $Q_6$  value of a perfect fcc lattice. Below each region, we illustrate the phase with a corresponding snapshot. Note that at the lowest temperature, we see signs of phase separation.

regime where the system remains fluid, it is likely that the thermodynamically stable phase is crystalline but that its formation is prevented on the time scales accessible to our simulations. However, for the purposes of designing a good glass former, the observation that the system does not crystallize on the longest possible simulation run-time is sufficient: many traditional glass forming models have been shown to have a stable crystal phase in the temperature regime of interest (see, e.g., Refs. 16 and 67–69).

In Fig. 2(a), we show the structure factor of the SW system for the low temperature crystal and for a liquid at intermediate temperature. The structure factor of the SW liquid displays the standard features of a simple liquid, and therefore, it will be our reference point of a “normal” liquid. As one might expect, the crystal phase presents strong peaks at specific wavelengths due to the translational order in the crystal. Note that the high degree of noise in the  $S(q)$  is related to the defects and dislocations in the (spontaneously formed) crystal. In Figs. 2(b) and 2(c), we show the structure factor in the  $xy$ -plane

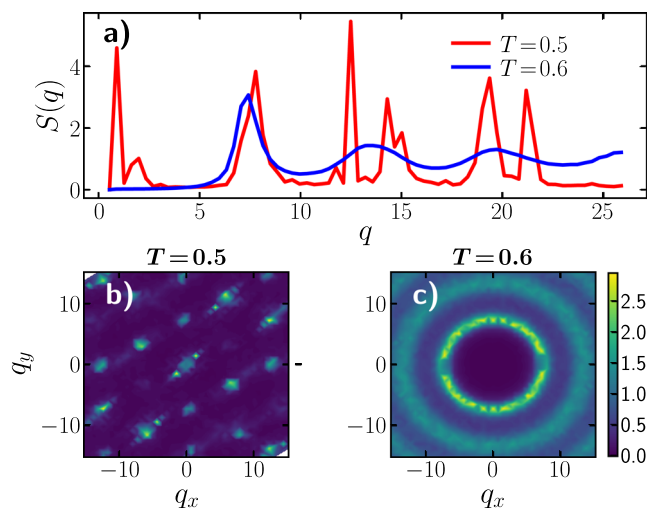


**FIG. 2.** (a) Structure factor of the square-well system with potential range of  $r_e = 1.03\sigma$  of a crystallized system at  $T = 0.5$  and a liquid system at  $T = 0.6$ . (b) Projection of the structure factor of the same crystallized system in the plane  $xy$ . (c) Projection for the corresponding liquid state.

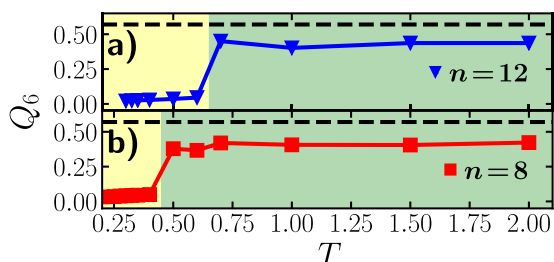


**FIG. 3.**  $Q_6$  as a function of temperature for the two patchy cases: (a)  $n = 12$  patches and (b)  $n = 8$  patches at a packing fraction corresponding to  $\eta = 0.56$ . Yellow regions correspond to a fluid phase and green regions to a crystallized phase, and dashed line is the  $Q_6$  value of a perfect fcc lattice.

for the crystal and the liquid, respectively. Indeed, the anisotropic ordering of the crystal phase is clearly visible in Fig. 2(b), whereas the liquid presents the usual ring pattern of a liquid [Fig. 2(c)].

## B. Patchy particle systems

We now turn our attention to the patchy models. First, we analyze the phase behavior of the monodisperse system with  $n = 12$  patches by calculating the  $S(q)$  for all investigated temperatures. As one might expect, at high temperatures, where the patches have little effect, the system still crystallizes into an fcc structure. However, upon cooling below  $T \leq 0.6$ , the directional attractions imposed by the patches allow the system to remain as a fluid for all remaining temperatures that were investigated. This phase behavior is reflected in the calculation of  $Q_6$  shown in Fig. 3(a). At low temperatures,  $Q_6$  is close to 0, while at higher temperatures, the corresponding values of  $Q_6$  are significantly higher, indicating crystallization. Clearly, the directional interactions effectively aid in suppressing crystallization. We attribute this to the changes in the local structure caused by the anisotropic interactions, which interfere with the crystallization mechanism. However, this does raise the question: does this mechanism enforce an “atypical” liquid structure? To answer this question, in Fig. 4, we show the structure factor of each of the temperatures

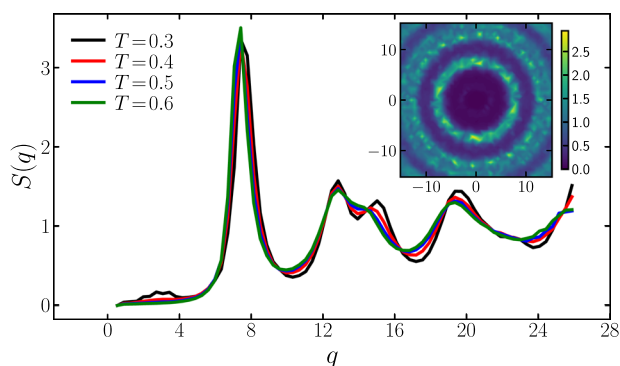


**FIG. 4.** Structure factor of the 12-patch system corresponding to temperatures where the system has not crystallized. The inset shows the projection of the structure factor in the  $xy$ -plane at  $T = 0.3$ .

where the system is in the fluid phase. In comparison to the isotropic case, the structure factor develops a split second peak upon cooling, a feature previously linked to icosahedral order.<sup>25</sup> This indeed indicates that the fluid structure undergoes strong changes due to the directionality imposed by the attractions, and in particular, it can be related to the formation of icosahedral clusters, as will be shown later on. These changes in the structure are strong enough to disrupt the formation of crystalline order.

To also explore a model that does not strongly enforce icosahedral order, we also have particles with  $n = 8$  patches. Similar to the previous case, the 8-patch particles also avoid crystallization in the low-temperature regime, although this regime is reached only for temperatures  $T \lesssim 0.4$  as shown in Fig. 3(b). However, the local structure of the 8-patch particles is much less strongly affected by the directional interactions than in the 12-patch case. We show in Fig. 5(a) the structure factor at the temperatures where the system is in a fluid phase. Note that in this case, we reach lower temperatures: as we will show later, the dynamics of the 8-patch system are faster than the 12-patch system at equal temperatures. The 8-patch structure factor shows a slight change as a function of temperature, suggesting that the structure remains close to that of a “typical” liquid. In particular, we do not observe a split of the second peak, and even at low temperatures, the structure factor remains highly similar to that of the square-well fluid (taken at the lowest temperature that avoids crystallization, see Fig. 5(b)).

To explore the structural features of these different models (8-patch, 12-patch, and SW) in more detail, we characterize their local structure.<sup>7</sup> We use the *Topological Cluster Classification* (TCC)<sup>55</sup> algorithm to detect the prevalence of different local clusters of particles in the fluid. In particular, we focus our attention to icosahedral and defective icosahedral clusters, which have both been linked to slow dynamics in glass formers.<sup>7,56–58</sup> In Figs. 6(a) and 6(b), we show the fraction of particles involved in icosahedral and defective icosahedral clusters, respectively, as a function of temperature for

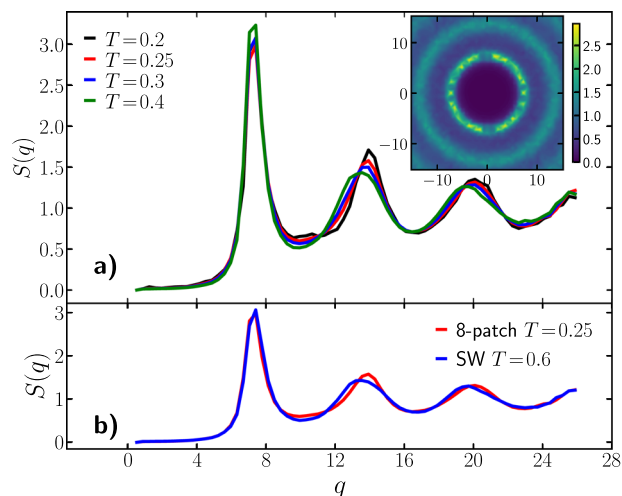


**FIG. 5.** (a) Structure factor of 8-patch fluids. The inset shows the two-dimensional structure factor in the  $xy$ -plane at  $T = 0.3$ . (b) Comparison between  $S(q)$  of the 8-patch system and a SW liquid.

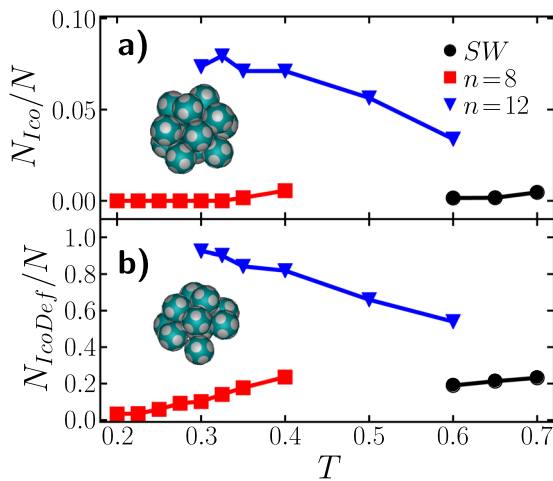


**FIG. 6.** (a) Fraction of particles in an icosahedral cluster as a function of temperature for the temperatures where the system is a fluid. (b) Fraction of particles in a defective icosahedral cluster. The inset shows an illustration of the icosahedral and defective icosahedral cluster, respectively.

the three studied cases. As expected, at low temperature, we find a sharp increase in the number of icosahedral clusters and defective icosahedral in the  $n = 12$  case. Indeed, in the 12-patch fluid at low temperatures, almost all particles are involved in at least one defective icosahedral cluster, which is likely linked to the strong changes in the structure factor. This is significantly higher than is typically observed in common glass forming models.<sup>7,70</sup> More importantly, as shown in the [supplementary material](#), the high concentration of icosahedral and other polytetrahedral local clusters strongly differentiate the 12-patch fluid from the metastable fluids of both the monodisperse SW model and simple hard spheres. In contrast, the 8-patch and the SW case show little icosahedral order, and this order tends to decrease with decreasing temperature. This demonstrates that while both the 8-patch and 12-patch geometries are able to avoid crystallization at sufficiently low temperatures, the two patch geometries have dramatically different effects on the local structure. Remarkably, none of the clusters captured by TCC become more prevalent when going to lower temperatures in the 8-patch case (see the [supplementary material](#)). By its nature, TCC only detects a limited number of local configurations (based on low-energy packings associated with several different model systems). Hence, any local structures that emerge in the 8-patch system are not ones that are detected by TCC. Nonetheless, the absence of strong changes in the structure factor suggests that the changes in the local structure made by the  $n = 8$  geometry are subtle in comparison to the  $n = 12$  case such that the overall liquid structure remains largely unchanged by going to lower temperatures. While there is no “ideal” structure for a glass former, the fact that the 8-patch system does not drastically disrupt the liquid structure, as the 12-patch system does, makes it a more attractive candidate as a monodisperse simple glass former. For this reason, the rest of this paper will be focused on a detailed characterization of the 8-patch model at different packing fractions.

### C. Detailed characterization of the 8-patch system

We now explore the thermodynamic and dynamic behavior of the 8-patch system in more detail. We start this investigation by measuring the temperature dependence of the energy and pressure for three different packing fractions ( $\eta = 0.56, 0.57,$  and  $0.58$ ). The results are shown in [Fig. 7](#). Note that at higher packing fractions, the system crystallizes for temperatures above  $T = 0.3$ . In the fluid phase, as shown in [Fig. 7\(a\)](#), the potential energy  $U$  of the system is not strongly dependent on the packing fraction. Note that the quantity  $U/N$  is exactly  $-1/2$  times the average number of bonds formed by a particle in the system. For all investigated packing fractions, the number of bonds increases monotonically as the temperature is reduced. At the lowest temperature, most particles are involved in at least six bonds ( $U/N < -3$ ), and around 20% of the particles are fully bonded, i.e., all eight of their patches are bonded to a neighbor. Although the potential energy of the system is still decreasing at the lowest investigated temperature for all packing fractions, some saturation of the number of bonds is visible, especially for  $\eta = 0.58$ . As such, it is not clear whether the bonding geometry of these particles permits the formation of a fully bonded disordered fluid state in the low-temperature limit.<sup>4</sup> In contrast, this system can, in principle, form at least one fully bonded crystal phase. In particular, using FBMC simulations,<sup>45</sup> we found fully bonded unit cells for crystal phases for packing fractions above  $\eta = 0.649$ . The densest version of this phase corresponds to a face-centered cubic (fcc) crystal, as shown in the inset of [Fig. 7\(a\)](#), which deforms into a body-centered tetragonal (BCT) structure at lower pressures. To examine the stability of this crystal structure at low temperatures, we performed simulations in which this crystal phase coexisted directly with a low-density fluid and estimated the coexistence density of both phases. Below a temperature of approximately  $T \approx 0.28$ , we indeed find a broad coexistence region, indicating that in the glassy regime, the fluid is indeed metastable with respect to

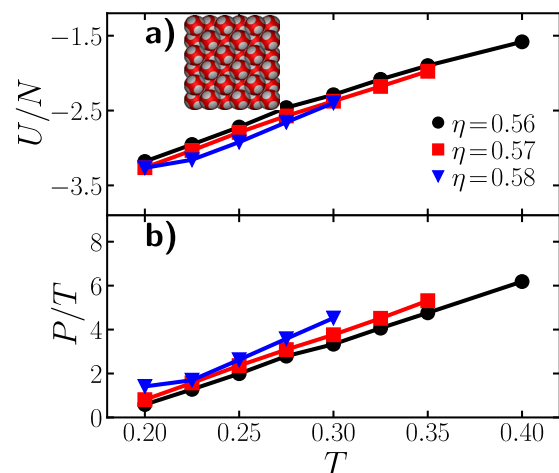


**FIG. 7.** (a) Average energy per particle as a function of temperature of the  $n = 8$  patches. Inset shows a fully bonded face-centered cubic crystal structure at close packing. Each particle is bonded to eight neighbors. (b) Dimensionless pressure, note that at temperatures lower than the ones studied here ( $T \approx 0.18$  or lower), the system might present phase separation.

crystallization. At higher temperatures, the coexistence region is expected to become more narrow, and other crystal phases (including plastic crystals) will take over. Since the details of the crystal phase are not relevant for the glassy behavior, we do not perform an exhaustive search here. In any case, from our simulations, it is clear that in the low-temperature regime, crystallization is kinetically avoided due to the strong dynamical slowdown induced by the patchy interactions.

In Fig. 7(b), we plot the pressure  $P$  for the same systems. As expected, the pressure decreases with decreasing temperature. A linear extrapolation to lower  $T$  (below the investigated range) would suggest that the pressure comes close to vanishing for  $T \approx 0.18$ , at least for the two lower packing fractions. This suggests that these isochores hit the gas–liquid binodal close to this temperature. Thus, for  $T < 0.18$ , at these two packing fractions, we expect the system to attempt to phase separate into coexisting gas and liquid phases. However, the extremely slow dynamics at these state points will likely lead to gelation. For the higher packing fraction  $\eta = 0.58$ , both the pressure and the energy level off near  $T = 0.20$ , and hence, this scenario may be avoided. Note that such a transition has also been noted for glassy binary mixtures of square-well particles<sup>71,72</sup> as well as for polydisperse systems.<sup>66</sup> The critical temperature associated with this binodal is strongly dependent on the range of the attraction.<sup>73</sup>

To locate the gas–liquid curve for our model, we use Successive Umbrella Sampling (SUS) simulations.<sup>48</sup> In Fig. 8, we show the gas–liquid coexistence and the estimated critical point corresponding to  $T_c = 0.1996$  and  $\eta_c = 0.26$ . Additionally, we draw in the same plot the estimated gas–crystal coexistences in the low-temperature regime, which we estimate from direct coexistence simulations starting from a seed of the fully bonded crystal from Fig. 7 placed in contact with a vacuum. Under these conditions, particles evaporate from the crystal surface until the chemical potential of the particles in the gas phase equals the one in the crystal phase. We find that

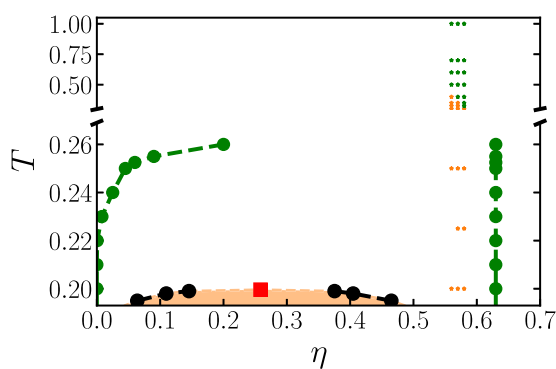


**FIG. 8.** Phase diagram of the 8-patch system. The gas–liquid region, obtained from successive umbrella sampling simulations, is colored in orange. The coexisting densities are marked by black filled circles, and the location of the critical point is marked by a red filled square. The low-temperature gas–crystal coexistence, estimated from direct coexistence simulations, is denoted with green circles. Green stars correspond to simulations where the system crystallizes, and orange ones correspond to simulations in the fluid phase.

both the gas–liquid binodal and the glassy regime occur in the part of the phase diagram that is metastable with respect to gas–crystal phase separation. Indeed, short-ranged attractive interactions tend to make the gas–liquid critical point metastable with respect to crystallization, as has been previously demonstrated for both SW<sup>74</sup> and patchy model systems.<sup>75</sup> Note that we here assume that the relevant crystal structure is the fully bonded one found in floppy box Monte Carlo simulations. While this assumption is reasonable in the limit of low temperatures, other crystal structures may appear at higher temperatures, resulting in shifts in the coexistence lines. However, any more stable crystal structure will only enlarge the gas–crystal coexistence region. The presence of other relevant crystal (or plastic crystal) phases becomes more likely with increasing temperature. As these structures are not relevant to the glassy behavior as long as the system remains fluid, we do not further explore crystallization here.

Despite the presence of a stable crystal phase, in the time window examined here, our systems behave as a metastable fluid. Indeed, many monodisperse and binary glass models have been shown to be metastable with respect to a crystalline or quasicrystalline phase.<sup>16,68,69</sup> However, within their metastable liquid phase, these systems still behave as good glass former.

In the phase diagram, we immediately note a large portion of the parameter space with  $T \leq T_c$  and  $\eta > \eta_c$  where a glassy (meta)stable liquid can be produced. The advantage of the directional patchy interaction aids in enlarging this region for two reasons: both by suppressing crystallization and by moving the location of the critical point to lower packing fractions and temperatures in comparison to isotropic interactions.<sup>76</sup>

Having obtained a clear idea of the location of the (meta)stable liquid region for the 8-patch case, we turn our attention to its dynamical behavior. To do so, we calculate the intermediate scattering function (ISF) and the mean-squared displacement (MSD). In Fig. 9(a), we show the MSD for a fixed packing fraction  $\eta = 0.56$

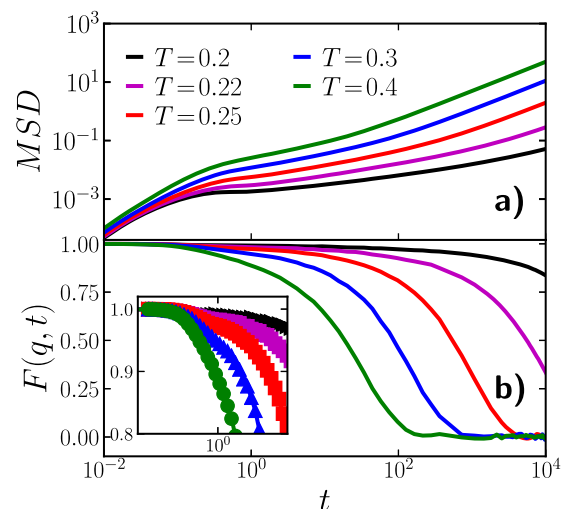


**FIG. 9.** (a) Mean-squared displacement of the 8-patch fluid at a fixed packing fraction  $\eta = 0.56$ . (b) Corresponding intermediate scattering function. The inset shows a close-up of the region where the first decay in the ISF happens.

and for some of the temperatures where the system is a fluid. As expected, at short times, the particles undergo ballistic motion. At intermediate times, the particles are caged and we observe the typical two-step relaxation of glassy fluids. Decreasing the temperature, however, we observe that the localization length decreases, as indicated by the reduced height of the plateau. This is a clear indication that the particles are strongly localized by the bonds with their neighbors.<sup>41</sup> Finally, at long time scales, the dynamics become diffusive. Note that the dynamics for the case  $T = 0.2$  are extremely slow, and the system did not fully relax on the time scale of our simulation. In Fig. 9(b), we plot the ISF. Even at this relatively low packing fraction, the system displays glassy behavior at all temperatures where the system is fluid, as evidenced by the two-step relaxation of the ISF. Note, however, that at low temperatures, the plateau in the ISF is very close to 1, again pointing at the strong localization of the particles at short time scales. As expected for a glass former, we see a dramatic increase in the structural relaxation time as the temperature is decreased. The behavior at higher packing fractions is qualitatively the same as the one at  $\eta = 0.56$  but shifted to longer time scales as the system goes deeper into the glassy regime.

In order to investigate the importance of collective rearrangements in the monodisperse glass, we calculate the self ISF and we compare it with the total ISF. From both intermediate scattering functions, we extract the relaxation times  $\tau_{0,3}$  and  $\tau_{0,3}^S$ , respectively, with the last one corresponding to the relaxation time extracted from the self ISF. In Fig. 10, we show both relaxation times for all the packing fractions and temperatures of the 8-patch case. The two relaxation times are consistently on the same order, suggesting that single-particle diffusion is the main driving force behind structural relaxation on the nearest neighbor length scale.

Consistent with the increasing relaxation times, the diffusion becomes slower as the packing fraction increases. In Fig. 11(a), we show the diffusion coefficient  $D$  calculated from the MSD through the Einstein diffusion equation,  $D = \lim_{t \rightarrow \infty} \frac{1}{6Nt} \langle \sum_{j=1}^N [r_j(t) - r_j(0)]^2 \rangle$ . Based on the diffusion coefficient, we define the diffusion time  $\tau_D = 1/D$ , associated with the typical time it takes a particle to diffuse one diameter. In Fig. 11(b), we plot this diffusion time against the collective relaxation time  $\tau_{0,3}$  for all the packing fractions studied and the temperatures where the

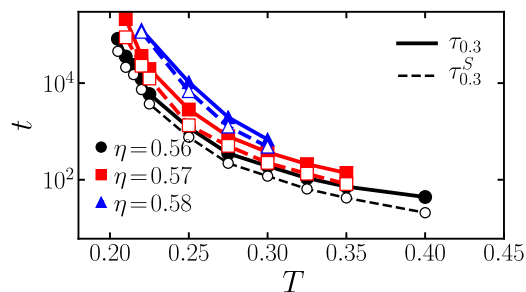


**FIG. 10.** Relaxation times of the  $n = 8$  case for all the investigated packing fractions. Dashed lines and empty symbols correspond to the ones extracted from the self-intermediate scattering function, and continuous lines correspond to the collective one. Both sets of data refer to  $q\sigma = 7.1$ .

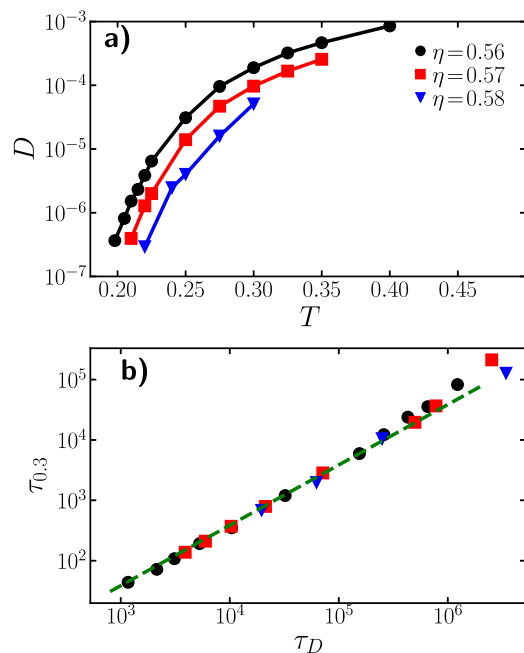


**FIG. 11.** (a) Dimensionless diffusion of the  $n = 8$  patch for different packing fractions. (b) Relaxation times  $\tau_{0,3}$  as a function of the diffusion time  $\tau_D$ .

system is in a fluid state. Interestingly, although the dynamics are extremely slow in all investigated systems, the two time scales grow at the same rate, consistent with the Stokes–Einstein relation. This is in contrast to most glass-forming liquids, where this relation tends to break down in the glassy regime.<sup>77,78</sup>

We note, however, that one downside of the model presented here is its relatively high computational expense. In comparison to, e.g., the isotropic square-well potential, simulating patchy particles comes at a significant additional computation cost. In particular, the simulation has to take into account the rotational motion of the particle and numerically predict collisions between the patches.<sup>4</sup> As a result, the simulations of patchy systems are approximately a factor 10–20 times slower than simulations of a comparable hard-sphere system, when we compare the time it takes to simulate one Brownian time unit  $\tau_B = \sigma\sqrt{m/k_B T}$ . This limits our ability to equilibrate the system deep inside the supercooled regime. Hence, we cannot exclude the possibility that the Stokes–Einstein relation will break down at deeper supercooling.

In order to better characterize the relaxation of the systems over different length scales, we also determine the behavior of the relaxation time  $\tau_{0,3}$  as a function of the wavelength  $q$ . The results are shown in Fig. 12(a), where we plot  $\tau_{0,3}(q)$  for the three different packing fractions and two different temperatures. The relaxation time shows a peak at the wavelength  $q$  corresponding to the first peak of the  $S(q)$ . This effect is in contrast with the one seen for binary mixtures where the low  $q$  limit is where the maximum of the relaxation time is attained as a mixing effect.<sup>15,79</sup> We clearly see here the advantage of having a monodisperse glass former where these mixing effects are not present.

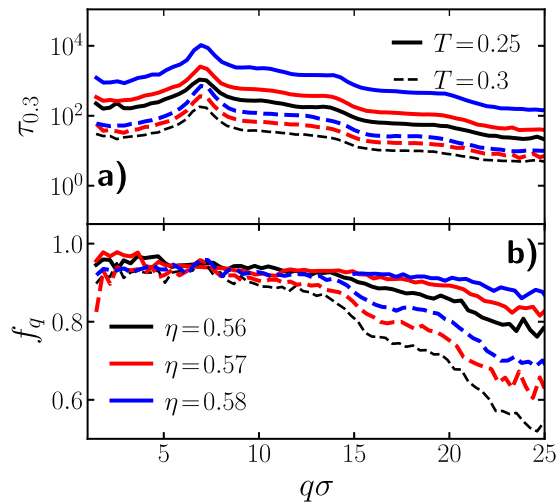


**FIG. 12.** (a) Collective relaxation time as a function of  $q$ -vector. Continuous lines correspond to  $T = 0.25$ , and dashed lines correspond to  $T = 0.3$ ; different colors correspond to different packing fractions  $\eta$ . (b) Corresponding non-ergodicity parameter.

Finally, more information about the nature of the glass can be obtained by the non-ergodicity parameter  $f_q$ . We show in Fig. 12(b) the  $f_q$  for the two lowest temperatures and packing fractions. Broadly speaking, the values of  $f_q$  are close to 1 over a wide range of length scales, indicating that the structure of the system is highly rigid until bonds start breaking. As one might expect, this is particularly true at the lowest temperature, where the number of bonds in the system is highest. This is a typical characteristic of an attraction driven glass, where the dynamical arrest of the system is driven by strong short-ranged attractions. However, it has been argued that attractive glasses are always an idealization and that in reality, they represent a transient regime of a repulsively dominated glass.<sup>41,66,80</sup> This regime, however, remains relevant under many experimental conditions due to its long relaxation time.

#### IV. CONCLUSIONS

We have exploited the anisotropic interactions of patchy particles to design a monodisperse glass former. In general, a good glass former preserves a liquid structure within large windows of relaxation times, while always avoiding crystallization. We have shown that this feature is fulfilled by a properly designed monodisperse system of patchy particles. In particular, we have explored the cases with  $n = 8$  and  $n = 12$  patches. The 8-patch system preserves a simple liquid-like structure factor deep into the glassy regime, in contrast to the 12-patch system that, while avoiding crystallization over a wider range of temperatures, presents a strong disruption of the local structure. For the 8-patch system, we also demonstrate that glassy behavior can be observed well before the gas-liquid binodal is reached. Hence, by properly choosing a patch geometry, we can simultaneously suppress crystallization and avoid phase separation at low temperatures and high densities. This opens up an extensive region of (meta)stable fluid where glass formation can be

observed in a monodisperse glass former. Moreover, this is achieved without the use of, e.g., oscillatory potentials or many-body interactions that would be exceedingly hard to realize in an experimental colloidal system. Hence, the 8-patch model may be an excellent candidate model for studying the glass transition by ruling out any effects that could occur in mixtures such as demixing, separation of time scales between the species, or formation of complex multicomponent crystals.

Finally, we note here that we have only explored two patch geometries that result in two glass formers with dramatically different local structures. For future work, it would be extremely interesting to explore the detailed effects of tuning, e.g., the placement and size of the attractive patches, both in order to optimize the resistance of the system to crystallization over a wide range of temperatures and to create ideal model systems for revealing the interplay between the local structure and dynamics in glassy systems.

#### SUPPLEMENTARY MATERIAL

See the [supplementary material](#) for more information about the structure of the 8-patch case.

#### ACKNOWLEDGMENTS

S.M.-A. acknowledges support from the Consejo Nacional de Ciencia y Tecnología (CONACyT, Scholarship No. 340015/471710).

#### DATA AVAILABILITY

The data that support the findings of this study are available from the corresponding author upon request.

#### REFERENCES

- <sup>1</sup>T. Palberg, E. Bartsch, R. Beyer, M. Hofmann, N. Lorenz, J. Marquis, R. Niu, and T. Okubo, *J. Stat. Mech.: Theory Exp.* **2016**, 074007.
- <sup>2</sup>W. F. Smith, J. Hashemi, and F. Presuel-Moreno, *Foundations of Materials Science and Engineering* (McGraw-Hill Publishing, 2006).
- <sup>3</sup>J. Russo, F. Romano, and H. Tanaka, *Phys. Rev. X* **8**, 021040 (2018).
- <sup>4</sup>F. Smallenburg and F. Sciortino, *Nat. Phys.* **9**, 554 (2013).
- <sup>5</sup>C. A. Angell, *J. Non-Cryst. Solids* **354**, 4703 (2008).
- <sup>6</sup>J. Taffs and C. P. Royall, *Nat. Commun.* **7**, 13225 (2016).
- <sup>7</sup>S. Marín-Aguilar, H. H. Wensink, G. Foffi, and F. Smallenburg, *Soft Matter* **15**, 9886 (2019).
- <sup>8</sup>W. Kob and H. C. Andersen, *Phys. Rev. E* **51**, 4626 (1995).
- <sup>9</sup>L. J. Lewis and G. Wahnström, *Phys. Rev. E* **50**, 3865 (1994).
- <sup>10</sup>E. Zaccarelli, S. M. Liddle, and W. C. K. Poon, *Soft Matter* **11**, 324 (2015).
- <sup>11</sup>W. Götze, *Complex Dynamics of Glass-Forming Liquids: A Mode-Coupling Theory* (OUP Oxford, 2008), Vol. 143.
- <sup>12</sup>G. Foffi, K. A. Dawson, S. V. Buldyrev, F. Sciortino, E. Zaccarelli, and P. Tartaglia, *Phys. Rev. E* **65**, 050802 (2002).
- <sup>13</sup>W. Götze and T. Voigtmann, *Phys. Rev. E* **67**, 021502 (2003).
- <sup>14</sup>G. Foffi, W. Götze, F. Sciortino, P. Tartaglia, and T. Voigtmann, *Phys. Rev. Lett.* **91**, 085701 (2003).
- <sup>15</sup>P. H. Handle, L. Rovigatti, and F. Sciortino, *Phys. Rev. Lett.* **122**, 175501 (2019).
- <sup>16</sup>P. K. Bommineni, N. R. Varela-Rosales, M. Klement, and M. Engel, *Phys. Rev. Lett.* **122**, 128005 (2019).

- <sup>17</sup>M. H. Bhat, V. Molinero, E. Soignard, V. C. Solomon, S. Sastry, J. L. Yarger, and C. A. Angell, *Nature* **448**, 787 (2007).
- <sup>18</sup>L. Zhong, J. Wang, H. Sheng, Z. Zhang, and S. X. Mao, *Nature* **512**, 177 (2014).
- <sup>19</sup>V. Molinero, S. Sastry, and C. A. Angell, *Phys. Rev. Lett.* **97**, 075701 (2006).
- <sup>20</sup>P. N. Pusey and W. van Meegen, *Nature* **320**, 340 (1986).
- <sup>21</sup>S. R. Williams and W. van Meegen, *Phys. Rev. E* **64**, 041502 (2001).
- <sup>22</sup>K. N. Pham, A. M. Puertas, J. Bergenholtz, S. U. Egelhaaf, A. Moussaid, P. N. Pusey, A. B. Schofield, M. E. Cates, M. Fuchs, and W. C. Poon, *Science* **296**, 104 (2002).
- <sup>23</sup>S. Auer and D. Frenkel, *Nature* **413**, 711 (2001).
- <sup>24</sup>R. Di Leonardo, L. Angelani, G. Parisi, and G. Ruocco, *Phys. Rev. Lett.* **84**, 6054 (2000).
- <sup>25</sup>M. Dzugutov, *Phys. Rev. A* **46**, R2984 (1992).
- <sup>26</sup>T. Mizuguchi and T. Odagaki, *Phys. Rev. E* **79**, 051501 (2009).
- <sup>27</sup>V. Van Hoang and T. Odagaki, *Physica B* **403**, 3910 (2008).
- <sup>28</sup>M. Engel and H.-R. Trebin, *Phys. Rev. Lett.* **98**, 225505 (2007).
- <sup>29</sup>M. Elenius, T. Oettel, and M. Dzugutov, *J. Chem. Phys.* **133**, 174502 (2010).
- <sup>30</sup>J. P. K. Doye, D. J. Wales, F. H. M. Zetterling, and M. Dzugutov, *J. Chem. Phys.* **118**, 2792 (2003).
- <sup>31</sup>A. Ikeda and K. Miyazaki, *Phys. Rev. Lett.* **106**, 015701 (2011).
- <sup>32</sup>Z. Gong, T. Hueckel, G.-R. Yi, and S. Sacanna, *Nature* **550**, 234 (2017).
- <sup>33</sup>J. S. Oh, G.-R. Yi, D. J. Pine *et al.*, *Proc. Natl. Acad. Sci. U. S. A.* **117**, 10645 (2020).
- <sup>34</sup>S. Ravaine and E. Duguet, *Curr. Opin. Colloid Interface Sci.* **30**, 45 (2017).
- <sup>35</sup>O. Marin, M. Alesker, S. Guttman, G. Gershinsky, E. Edri, H. Shpaisman, R. E. Guerra, D. Zitoun, M. Deutsch, and E. Sloutskin, *J. Colloid Interface Sci.* **538**, 541 (2019).
- <sup>36</sup>S. Marín-Aguilar, H. H. Wensink, G. Foffi, and F. Smallenburg, *J. Chem. Phys.* **152**, 084501 (2020).
- <sup>37</sup>J. N. Immink, J. J. E. Maris, P. Schurtenberger, and J. Stenhammar, *Langmuir* **36**, 419 (2019).
- <sup>38</sup>N. Kern and D. Frenkel, *J. Chem. Phys.* **118**, 9882 (2003).
- <sup>39</sup>The position of the patches in the  $n = 8$  case are:  $(-0.61, -0.61, -0.51)$ ,  $(-0.61, 0.61, -0.51)$ ,  $(0, -0.86, 0.51)$ ,  $(0, 0.86, 0.51)$ ,  $(0.61, -0.61, -0.51)$ ,  $(0.61, 0.61, -0.51)$ ,  $(-0.86, 0, 0.51)$  and  $(0.86, 0, 0.51)$ .
- <sup>40</sup>E. Zaccarelli, G. Foffi, K. A. Dawson, S. V. Buldyrev, F. Sciortino, and P. Tartaglia, *Phys. Rev. E* **66**, 041402 (2002).
- <sup>41</sup>E. Zaccarelli and W. C. K. Poon, *Proc. Natl. Acad. Sci. U. S. A.* **106**, 15203 (2009).
- <sup>42</sup>M. He, J. P. Gales, É. Ducrot, Z. Gong, G.-R. Yi, S. Sacanna, and D. J. Pine, *Nature* **585**, 524 (2020).
- <sup>43</sup>D. J. Kraft, R. Ni, F. Smallenburg, M. Hermes, K. Yoon, D. A. Weitz, A. van Blaaderen, J. Groenewold, M. Dijkstra, and W. K. Kegel, *Proc. Natl. Acad. Sci. U. S. A.* **109**, 10787 (2012).
- <sup>44</sup>L. Hong, A. Cacciuto, E. Luijten, and S. Granick, *Langmuir* **24**, 621 (2008).
- <sup>45</sup>L. Filion, M. Marechal, B. van Oorschot, D. Pelt, F. Smallenburg, and M. Dijkstra, *Phys. Rev. Lett.* **103**, 188302 (2009).
- <sup>46</sup>G. Doppelbauer, E. G. Noya, E. Bianchi, and G. Kahl, *Soft Matter* **8**, 7768 (2012).
- <sup>47</sup>T. Vissers, Z. Preisler, F. Smallenburg, M. Dijkstra, and F. Sciortino, *J. Chem. Phys.* **138**, 164505 (2013).
- <sup>48</sup>P. Virnau and M. Müller, *J. Chem. Phys.* **120**, 10925 (2004).
- <sup>49</sup>J. Russo, J. Tavares, P. Teixeira, M. T. da Gama, and F. Sciortino, *Phys. Rev. Lett.* **106**, 085703 (2011).
- <sup>50</sup>L. Rovigatti, J. M. Tavares, and F. Sciortino, *Phys. Rev. Lett.* **111**, 168302 (2013).
- <sup>51</sup>F. Smallenburg and F. Sciortino, *Phys. Rev. Lett.* **115**, 015701 (2015).
- <sup>52</sup>L. Rovigatti, J. Russo, and F. Sciortino, *Phys. Rev. Lett.* **107**, 237801 (2011).
- <sup>53</sup>P. J. Steinhardt, D. R. Nelson, and M. Ronchetti, *Phys. Rev. B* **28**, 784 (1983).
- <sup>54</sup>Y. Wang, S. Teitel, and C. Dellago, *J. Chem. Phys.* **122**, 214722 (2005).
- <sup>55</sup>A. Malins, S. R. Williams, J. Eggers, and C. P. Royall, *J. Chem. Phys.* **139**, 234506 (2013).
- <sup>56</sup>F. C. Frank, *Proc. R. Soc. London, Ser. A* **215**, 43 (1952).
- <sup>57</sup>M. Leocmach and H. Tanaka, *Nat. Commun.* **3**, 974 (2012).
- <sup>58</sup>C. P. Royall and W. Kob, *J. Stat. Mech.: Theo. Exp.* **2017**, 024001.
- <sup>59</sup>V. J. Anderson and H. N. W. Lekkerkerker, *Nature* **416**, 811 (2002).
- <sup>60</sup>P. Bolhuis, M. Hagen, and D. Frenkel, *Phys. Rev. E* **50**, 4880 (1994).
- <sup>61</sup>S. Buzzaccaro, R. Rusconi, and R. Piazza, *Phys. Rev. Lett.* **99**, 098301 (2007).
- <sup>62</sup>G. Foffi, G. D. McCullagh, A. Lawlor, E. Zaccarelli, K. A. Dawson, F. Sciortino, P. Tartaglia, D. Pini, and G. Stell, *Phys. Rev. E* **65**, 031407 (2002).
- <sup>63</sup>E. Zaccarelli, H. Löwen, P. Wessels, F. Sciortino, P. Tartaglia, and C. Likos, *Phys. Rev. Lett.* **92**, 225703 (2004).
- <sup>64</sup>F. Sciortino, *Nat. Mater.* **1**, 145 (2002).
- <sup>65</sup>L. Cipelletti and L. Ramos, *J. Phys.: Condens. Matter* **17**, R253 (2005).
- <sup>66</sup>C. P. Royall, S. R. Williams, and H. Tanaka, *J. Chem. Phys.* **148**, 044501 (2018).
- <sup>67</sup>T. S. Ingebrigtsen, J. C. Dyre, T. B. Schröder, and C. P. Royall, *Phys. Rev. X* **9**, 031016 (2019).
- <sup>68</sup>J. Roth, *Phys. Rev. Lett.* **79**, 4042 (1997).
- <sup>69</sup>S. Toxvaerd, U. R. Pedersen, T. B. Schröder, and J. C. Dyre, *J. Chem. Phys.* **130**, 224501 (2009).
- <sup>70</sup>J. E. Hallet, F. Turci, and P. Royall, *Nat. Commun.* **9**, 3272 (2018).
- <sup>71</sup>G. Foffi, C. De Michele, F. Sciortino, and P. Tartaglia, *Phys. Rev. Lett.* **94**, 078301 (2005).
- <sup>72</sup>G. Foffi, C. D. Michele, F. Sciortino, and P. Tartaglia, *J. Chem. Phys.* **122**, 224903 (2005).
- <sup>73</sup>J. Largo, M. A. Miller, and F. Sciortino, *J. Chem. Phys.* **128**, 134513 (2008).
- <sup>74</sup>D. L. Pagan and J. D. Gunton, *J. Chem. Phys.* **122**, 184515 (2005).
- <sup>75</sup>F. Romano, E. Sanz, and F. Sciortino, *J. Phys. Chem. B* **113**, 15133 (2009).
- <sup>76</sup>E. Bianchi, J. Largo, P. Tartaglia, E. Zaccarelli, and F. Sciortino, *Phys. Rev. Lett.* **97**, 168301 (2006).
- <sup>77</sup>M. Dzugutov, S. I. Simdyankin, and F. H. M. Zetterling, *Phys. Rev. Lett.* **89**, 195701 (2002).
- <sup>78</sup>G. Tarjus and D. Kivelson, *J. Chem. Phys.* **103**, 3071 (1995).
- <sup>79</sup>G. Foffi, W. Götzke, F. Sciortino, P. Tartaglia, and T. Voigtmann, *Phys. Rev. E* **69**, 011505 (2004).
- <sup>80</sup>C. J. Fullerton and L. Berthier, "Glassy behaviour of sticky spheres: What lies beyond experimental timescales?" *Phys. Rev. Lett.* **125**(25), 258004 (2020).